EARTH OBSERVATION AND GEOMATICS ENGINEERING
website: https://eoge.ut.ac.ir

Quantitative Assessment of the Trends and Spatio-Temporal Variability of Vegetation Growth in Iran using Wavelet Transform and Statistical Approaches

Mojtaba Zoljoudi [1], Karim Naghdi [2 *], Masoud Moradi[3], Masoud Taefee Feijani [4]

[1]Department of Marine Meteorology & Physical Oceanography, Atmospheric Science & Meteorological Research Center
[2]Department of Surveying Engineering, Islamic Azad University, Taft Branch, Taft, Yazd, Iran
[3]Iranian National Institute of Oceanography and Atmospheric Science
[4]Aerospace Research Institute (Ministry of Science, Research and Technology)

Article history:
Received: 2021-12-25, Received in revised form: 2022-05-25, Accepted: 2022-05-30

ABSTRACT

In this research, the Spatio-temporal variability of vegetation growth was evaluated using Moderate Resolution Imaging Spectroradiometer (MODIS) Level 3 Enhanced Vegetation Index (*EVI*) at 1km resolution data products during 2003-2018 over Iran. The total variability, the amplitude of the annual phenological cycle, seasonal cycle peak, inter-annual variation, minimum level of variations, the timing of maximum vegetation, coefficient of variations, Sen's slope, Mann-Kendall and Hurst exponent indices were calculated as independent variables for all pixels. The results indicated that the variations of inter-annual cycles show a relatively stable trend, and relatively flat trend curves were observed for all types of vegetation in Iran. The seasonal phenological cycles were the most sources of intra-annual variations, and the maximum and minimum values were observed in mid-summer and early winter, respectively. The *EVI* peaks were observed in spring and summer and spatially have been distributed in 30.2% and 20.6% of the total areas. More than 44% of the total area showed stable vegetation coverages, and 1.7% of the total area showed a large amplitude of vegetation variations. About 89% of vegetated areas (37.7% of the total area) in the north, west, and southwest regions show improved sustainable variations with positive changes. The results show that about 5.5% of the vegetation coverage in the northeast and southwest decreased. The presented analytical indices in this research are a cost-effective method for managing and predicting future environmental trends in developing regions at risk of desertification.

KEYWORDS

MODIS,
Enhanced Vegetation Index,
Mann-Kendall Test,
Hurst Exponent,
Land Cover

1. Introduction

Iran has experienced frequent droughts and land degradation during the last three decades due to climate change and human activities (Emadodin et al., 2012; Madani et al., 2016). Several studies attempted to assess and monitor the effect of droughts and land degradation on vegetation coverage in some regional parts of Iran (Abdi et al., 2018; Ahmadi & Nusrath, 2010; Amiri et al., 2009; Golian et al., 2015; Kazemzadeh & Malekian, 2016; Sagheb-Talebi et al., 2014; Zoljoodi & Didevarasl, 2013). However, land degradation and land cover change in large areas are serious challenges in Iran (Emadodin et al., 2012; Rahimi et al., 2013). Knowledge about land degradation and land cover

* Corresponding Author
E-mail addresses: k_naghdi2002@yahoo.com (K. Naghdi)

changes is needed for sustainable land use management.

Studies on vegetation coverage are a key point for understanding regional ecosystems. In addition, Decreasing the vegetation index is a pre-sign of land degradation and desertification (Higginbottom & Symeonakis, 2014; Wessels et al., 2012, 2008). The lack of data and robust methods noted by several Iranian investigations means that comprehensive nationwide studies that consider vegetation trends in Iran are scant. As a research example, Eskandari et al. (2021) investigated desertification trends in Iran for the period 2001 to 2015 via a combination of normalized difference vegetation index (*NDVI*), net primary production (NPP), and leaf area index (*LAI*) as vegetation indices and precipitation and land surface temperature (*LST*) as climate indices. They combined these indices to analyze and map areas that are susceptible to land degradation.

To understand the variations of vegetation growth, it is required to know the inter-annual and seasonal variations (Detsch, Otte, Appelhans, Hemp, et al., 2016; Jiang et al., 2015). Vegetation Indexes (*VI*) extracted from Moderate Resolution Imaging Spectrometer (MODIS), such as *NDVI* (Beck et al., 2006; Cihlar et al., 1991; Fu et al., 2014; Jiang et al., 2015), Enhanced Vegetation Index (*EVI*) (Moreira et al., 2019; Pan et al., 2012; Sims et al., 2006; X. Zhang et al., 2003), and NPP (Y. Zhang et al., 2009; Zhao et al., 2005) have been used widely for vegetation phenology studies. *NDVI* is the most utilized vegetation index to monitor vegetation dynamics processes (Fensholt & Proud, 2012; Martínez & Gilabert, 2009; Song, F.Q. et al., 2011). *EVI* also has been used to study vegetation phenology and its Spatiotemporal dynamics. *EVI* is more sensitive to the *LAI* and architecture of the canopy in comparison with *NDVI* (Huete et al., 2002; Rocha & Shaver, 2009; Van Leeuwen et al., 2013). It is an efficient index for studying vegetation phenology in different scales of time and space (Cao et al., 2015; Tan et al., 2011). In particular, Zhang et al. (2017) reanalyzed the MODIS-C5 and MODIS-C6 VI datasets and found that due to sensor degradation in MODIS-C5, it is recommended to use MODIS-C6 datasets for vegetation studies. Also, it has been denoted that there is a strong association between climate and vegetation in arid regions based on MODIS Terra-C6 *EVI* datasets (Detsch, Otte, Appelhans, & Nauss, 2016; Y. Zhang et al., 2017). Therefore, *EVI* datasets from MODIS Terra-C6 can reflect the Spatiotemporal characteristics of land surface vegetation, and also could be used as an efficient factor for monitoring vegetation variations.

VI signals are characterized by inter-annual and intra-annual variations, and usually indicate non-stationary processes (Bradley et al., 2007; Martínez & Gilabert, 2009). Spectral frequency techniques that work in the time domain are required to extract information from this type of time-series dataset. Wavelet Transform (WT) is a well-developed methodology for stationary and non-stationary time-series data analysis. The non-stationary signals are distributed irregularly, and WT enables us to decompose them to different scales of frequency and time (Percival et al., 2004). WT approach has been applied to VI time series analysis for vegetation dynamics, change detection, and phenology studies (Bruce et al., 2006; Carl et al., 2013; Martínez & Gilabert, 2009; Moreira et al., 2019; Percival et al., 2004; Piao et al., 2012). All of these studies demonstrate the potential of WT analysis for vegetation dynamics and variations studies.

Inter-annual variations of the *VI* series usually show non-linear trends (Peng et al., 2012; Shuang-cheng et al., 2008). Linear regression analysis often has been used for trend analysis in vegetation studies because of its simplicity (Fensholt et al., 2009). Further, the regression slope and correlation coefficient do not affect linear regression. Instead, it is assessed or judged by it. For the use of linear regression, the data distribution should follow the normal distribution, which may not be the case always. In such a situation, non-parametric trends such as Sen's Slope and Mann-Kendall test give rise to better results. Non-parametric trends can also accommodate data gaps, short time series, and outliers. Therefore, The Sen's Slope and Mann-Kendall test could be more efficient for *VI* inter-annual trend analysis (Jiang et al., 2015; Martínez & Gilabert, 2009; Peng et al., 2012). In addition, the consistency of the VI inter-annual series in nature is an important factor that determines the stability of the variations trend. The Hurst exponent has been used to quantify the sustainability of time series data and has been used in many studies for vegetation trend analysis and prediction (Hou et al., 2012; Jiang et al., 2015; Peng et al., 2012). Although the Hurst exponent is an efficient index to determine the duration of trends, it could not predict the duration of the sustainability of the predicted trends.

In this study, the vegetation dynamics and trends of variations were analyzed using MODIS Terra *EVI* during 2003-2018 in Iran. The wavelet transform technique was used to extract intra-annual and inter-annual series characteristics, Sen's Slope test to assess the magnitude of the trend and Man-Kendall test to assess the presence of any trend, and the Hurst exponent was implemented for trend analysis and detection of persistence of variations. To achieve this, some samples were selected from different vegetation classes, and analyses were applied to them to find the best key features which represent the *VI* variability and trends. Finally, the approved methodologies and key features were implemented on all pixels of the whole image. This study aimed to investigate the temporal and spatial variations, fluctuations, temporal trends, and sustainability of the vegetation coverage changes in Iran, where there is a lack of data about vegetation distribution and variation at the country level.

2. Study Area

Iran is one of the largest countries in the middle-east with an arid to semi-arid climate in general (Modarres & da Silva, 2007). It borders the Caspian Sea in the north and the Persian Gulf and Oman Sea in the south. Iran is a country on the central plateau with mountains in the north, north-west, west, and south-west. Its area is about 1.6 million square kilometers. Elevation ranges from ~-28 m along the Caspian Sea in the north, up to more than 5700m at Damavand mountain in central-north. Because of topography, geographical location, and distance from the sea, the climate regime shows a gradient from warm and dry in the southeast, humid and warm in the north, to cold and humid in the northwest. Central and eastern parts of Iran are dominated by a desert plateau called Dasht-e-Kavir which is one of the hottest places on earth. In the south, winters are moderate and summers are very hot, with an average daily temperature in July ~38°C. Whereas, in the northwest part, winters are cold with heavy snowfall and subfreezing temperatures during December and January. Annual precipitation varies from less than 100 mm in most of the country, and up to 1000 mm along the Caspian Sea (Madani et al., 2016) .

Based on topography and climate features in Iran, four ecological zones (Iran-o-Touranian zones, Zagros, Khalij-o-Omani, and Hyrcanian) with specific plant richness from the highest area to the lowest area were established respectively. The lowest plant diversity is in the Khalij-o-Omanian zone in the southern part of Iran, which is a flat area. In contrast, the Hyrcanian zone is rich in biodiversity with 8000 plant species representative of many different life forms (Herb, Grass, Shrub, and tree) in the northern part of Iran (Eftekhari, T., Ramezani, M., 2004). Climatological and hydrological aspects of Iran control the spatial differentiation of vegetation types. The most extensive growth area and forest are located in the north along the Caspian Sea in a completely different climate close to subtropical conditions. About 7% of Iran is forested, and 58% of the total area is barren lands. The dominant vegetation covering Iran are low-growing plants such as grass, shrub, and trees. The distribution and richness of vegetation covers are controlled by climate and topography, which play important role in the biodiversity of this country (Heshmati, 2012). Fig. 1 shows the land cover map of Iran from "MODIS Terra and Aqua Combined Land Cover".

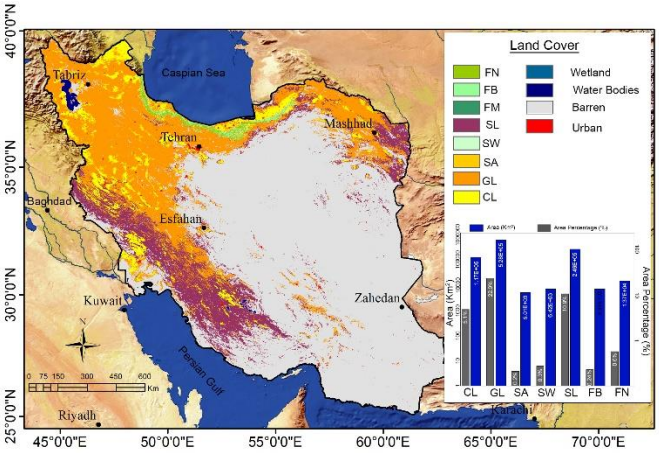

Figure 1. Land cover map of Iran. Data from NASA LPDAAC, MODIS yearly L3 global 500 m grid (MCD12Q1). Map classified based on International Geosphere-Biosphere Program (IGBP) classification schema. FN: Needleleaf Forest, FB: Broadleaf Forest, FM: Mixed Forest, SL: Closed Shrub, WS: Woody Savana, SA: Savanna, GL: Glass Land, CL: Crop Land. The lower-right graph shows the area of vegetation classes.

3. Data and Methods

3.1. Datasets

In this study, the MOD13A1 (Didan, K., 2015) V006 16-days *VI* composite at 1 km resolution from MODIS-Terra Level-3 was used. The MODIS datasets were downloaded from NASA Land Processes Distributed Active Archive Center (LPDAAC, http://lpdaac.usgs.gov/) for the period 2003 - 2018. Each of the MODIS datasets contains *NDVI*, *EVI*, and *VI* quality details, composite day of the year, and pixel reliability. Data were prepared in three steps before analysis. a) The snow/Ice, and high aerosol marked pixels were filtered using *VI* quality assessment layer flags. b) Cloud removal using 'pixel reliability summary' data layer, for all pixels ranked 'cloudy'. Some cloudy pixels are present in MODIS-L3 products, which are present mainly at the edge of bigger cloud patches. These suspicious pixels were identified using the method introduced by Hyndman et al. (2018) and were masked if falling inside a 3×3 focal matrix applied to each of the rejected pixels (Detsch, Otte, Appelhans, Hemp, et al., 2016). c) *EVI* temporal signals were smoothed and gaps refilled utilizing interpolation algorithms (Eerens et al., 2014; Swets et al., 1999). Pixels with more than 50% gaps in total time-series length were discarded. Next, the gaps in the *Chl-a* signals were filled using the DCT-PLS method (Garcia, 2010). This method utilizes

information from both time and space, uses a least square regression, and performs cosine transform for the smoothing of data in one and higher dimensions. It produces uninterrupted Spatio-temporal distributions, and it is not sensitive to outliers. It has been successfully used for filling the gaps in satellite-derived vegetation indices datasets (Bashmachnikov et al., 2013; Wang et al., 2012). Furthermore, *EVI* signals were smoothed in the time domain using the Savitzky-Golay filter with the 2nd order 7-point. This method preserves the area under the graph and effectively reduces high-frequency noises (Ziegel et al., 1987).

Land cover data were obtained from NASA LPDAAC, MODIS yearly L3 global 500 m grid (MCD12Q1). In this study, the International Geosphere-Biosphere Program (IGBP) classification schema of MODIS land cover has been used. The IGBP scheme identifies 17 land cover classes, which include 11 natural vegetation, and 6 non-vegetated classes. This product also provides quality control information and QC flags for all pixels (Friedl et al., 2010).

3.2. Methods

The Spatiotemporal variations of vegetation growth were evaluated using MODIS *EVI* at 1km resolution data products. The EVI is defined as (Moreira et al., 2019):

$$EVI=G\frac{NIR-Red}{NIR+C_1*Red-C_2*Blue+L} \quad (1)$$

where C_1 and C_2 are the aerosol resistance coefficients, and G is a gain factor. L is the canopy background adjustment for correcting the nonlinear, and *Blue*, *Red*, and *NIR* are atmospheric-corrected surface reflectances. In the MODIS EVI algorithm, the coefficients adopted are C_1=6, C_2=7.5, G=2.5, and L=1.

The trends of vegetation growth were calculated using wavelet transform coefficients and statistical approaches. The proposed methodology is shown in Fig. 2, and details were explained in the following sections.

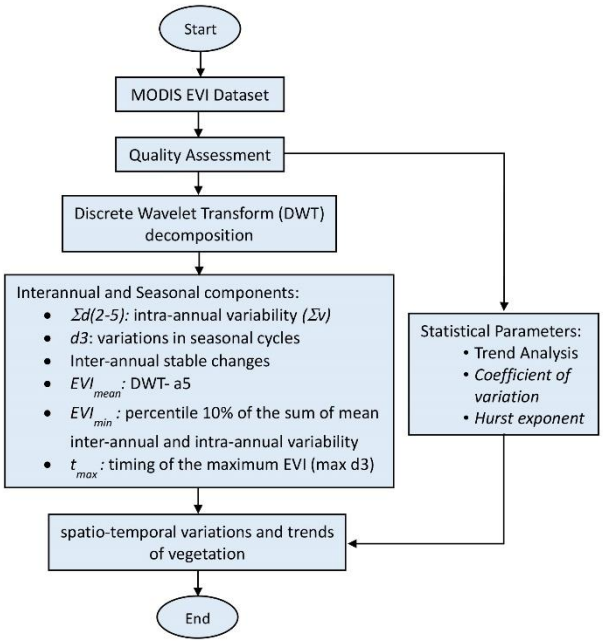

Figure 2. Flowchart of the research

3.2.1. Wavelet analysis

The main idea of wavelet analysis is the decomposition of the original signal into varying wavelet functions, called "mother-wavelet". This method decomposes a signal at different spatial or time scales into a hierarchical structure of details and approximations at limited levels. The original signal is decomposed into detail coefficients and approximation coefficients. (Percival & Walden, 2006). The approximation coefficients represent the low-frequency components of a signal, whereas the detail coefficients represent the high-frequency components. A basic characteristic of the wavelet analysis is a new parameter called "scale" which displays the frequency. According to that, the "time-scale representation" is introduced in wavelet analysis. The "scale" is the main parameter of wavelet analysis for non-stationary signals. High values of scaling are proportional to small values of frequency and vice-versa. In wavelet theory, instead of the parameter of time is used the parameter of "shift" is used.

In this study, the Discrete Wavelet Transform (DWT) analysis technique was used to evaluate the Spatiotemporal stability and anomaly of the *EVI* time series. DWT components are performed using dilated and shifted versions of the mother wavelet to produce a set of wavelet basis functions. Several mother wavelets are available for WT signal decompositions (e.g. Daubechies wavelet, 'db5', and Meyer orthogonal, 'dmey') application in environmental studies. In this study, the Meyer WT was used as a mother wavelet, because it has demonstrated successful results in land-cover changes analysis from MODIS time-series data (Echer, 2004; Freitas & Shimabukuro, 2008; Martínez & Gilabert, 2009). The Meyer wavelet as a type of continuous

wavelet is an orthogonal wavelet proposed by Yves Meyer.

Detection of inter-annual and intra-annual components of temporal data depends on the corresponding period in DWT analysis. The appropriate period is calculated based on the scale and frequency of original signals (Meyer, 1993):

$$p=a_j \Delta t/\upsilon_c \quad (2)$$

where: a_j is the scale, Δt is the sampling cycle ($\Delta t=16$ *days*), and ν_c is the central frequency of the wavelet.

Table 1 shows the corresponding temporal scales for the Meyer wavelet with a sampling cycle of 16 days and ν_c = 0.67213. The DWT components show the differences between temporally adjacent averages over the time range at different scales (Martínez & Gilabert, 2009).

Table 1. Period (p) and semi-period (p/2) of different decomposition levels (1 to 5) of DWT using the Meyer mother wavelet, and a sampling cycle of 16 days, νc = 0.67213.

Level (j)	Scale (a_j)	Period (days)	Semi-Period (days)	Change Detection (days)	Description
1	2	48	24	d1 (1-24)	sub-monthly
2	4	95	48	d2 (25-48)	monthly
3	8	190	95	d3 (49-95)	seasonal
4	16	381	191	d4 (96-191)	inter-seasonal
5	32	762	381	d5 (192-381)	inter-annual

Thus, inter-annual and intra-annual components can be interpreted as semi-period (half-period time p/2) time scales, which represent the differences between years and months, respectively. The approximation component for level 5, (j=5, a_5), allows detection of the changes over time scales of 381 days and longer, which provide information about the inter-annual variability or annual changes. In contrast, detail components (d1 to d5) with semi-period 24 to 381 days, are appropriate to analyze the intra-annual variability or monthly changes. Therefore, detail components (d1 to d5) can be used to detect changes at scales: d1(1-24 days), d2(25-48 days), d3(49-95 days), d4(96-191 days), d5(192-381 days), which correspond to sub-monthly, monthly, seasonal, inter-seasonal and inter-annual changes, respectively. The first level of variations represents the changes in less than 1 month and is considered temporal noise. DWT components represent some key features that have been used for vegetation dynamic studies (Hawinkel et al., 2015; Martínez & Gilabert, 2009; Roerink et al., 2003). The most important key features are:

1) sum of detail components 2-5 is considered as the total intra-annual variability (Σv). The amplitude of the annual phenological cycle is in the range of percentile 10% and 90% of the total intra-annual variability (ΔEVI). The amplitude of the phenological cycle relative to the average *EVI* ($\Delta EVI\%$) is more effective than ΔEVI and indicates the level of vegetation homogeneity during the desired period.

2) detail component 3 (with semi-period=95 days) can be related to variations of seasonal cycles.

3) the 5th approximation component describes the inter-annual stable changes and is considered as the mean *EVI* level of vegetation during the period (EVI_{mean}).

4) Minimum *EVI* (EVI_{min}) level during the period is defined as the percentile 10% of the sum of mean inter-annual and intra-annual variability.

5) The timing of the maximum *EVI* corresponding to the d3 component represents the phenological cycle of each vegetation cover type and is expressed as EVI_{max}.

3.2.2. Trend Analysis

Statistical trend tests are more effective tools than linear regression methods for trend analysis in long-time series datasets (De Beurs & Henebry, 2005). The Mann-Kendall test and Sen's Slope trend analysis have been widely used for detecting vegetation variation trends from long-time series datasets (Fensholt & Proud, 2012; Jiang et al., 2015; Lunetta et al., 2006; Martínez & Gilabert, 2009). The Mann–Kendall test as the non-parametric statistical test has been often used to measure the significance of trends in time series. The Mann–Kendall statistical test is calculated as (Eskandari et al., 2021):

$$S=\sum_{i=1}^{n-1}\sum_{j=i+1}^{n} \mathrm{sgn}(x_j-x_i) \quad (3)$$

where: x_i and xj are the data values in the time series i and j ($j>i$), respectively, $sgn(x_j - x_i)$ is the sign function, and n is the number of data points. If n is bigger than 8, statistic S approximates to normal distribution.

$$\mathrm{sgn}(x_j-x_i)=\begin{cases}+1 & \text{if } x_i-x_j>0\\ 0 & \text{if } x_i-x_j=0\\ -1 & \text{if } x_i-x_j<0\end{cases} \quad (4)$$

In this study, the Mann-Kendall statistical test was calculated with a confidence level of 95% using MATLAB®. The Tau-b coefficient is a measure of associations and ranges from -1 to +1. Values around zero show the absence of association, and fluctuations toward +1 and -1 values correspond to positive and negative associations, respectively. The 'h' coefficient and two-sided p-value represent the significance (h=1, p-value<0.05) or non-significance ($h=0$) of trends. Besides, the magnitude of a time series trend was calculated by a simple non-parametric

method proposed by Sen (1968). The Sen's slope is estimated by:

$$\beta = Median\left(\frac{x_i - x_j}{i - j}\right), \quad 1 \leq i < j \qquad (5)$$

Where β is Sen's slope estimate. $\beta > 0$ indicates an upward trend in a time series. Otherwise, the data series presents a downward trend during the period.

3.2.3. Coefficient of variation

The coefficient of variation (CV) represents the relative variability and is the ratio of the standard deviation to the average of datasets (Tucker et al., 1991). A large value of CV indicates that the time series datasets show larger fluctuations, and smaller values represent a more stable dataset. It is calculated by:

$$CV = \sigma EVI / Avg(EVI) \qquad (6)$$

where CV refers to the coefficient of variation of the *EVI* values of each pixel during 2003-2018. σEVI and Avg(*EVI*) represent the standard deviation and average of the EVI series of each pixel, respectively.

3.2.4. Hurst Exponent

The Hurst exponent (H) was originally developed in hydrological studies of the Nile river (Hurst, 1951). It has been used for vegetation variations trend studies in recent years (Fan et al., 2012; Hou et al., 2012; Jiang et al., 2015). The Hurst exponent (H) referred to as the "index of long-range dependence" or "index of dependence" is defined in terms of the asymptotic behavior of the rescaled range as a function of the time range of a time series as follows;

$$E\left[\frac{R(n)}{S(n)}\right] = C_n^H \text{ as } n=1, 2, \ldots, n\rightarrow\infty \qquad (7)$$

where: *n* is the number of data points in a time series, *R(n)* is the range of the first *n* cumulative deviations from the mean, *S(n)* is the series (sum) of the first n standard deviations, *C* is a constant, E*[x]* is the expected value, and *H* is the Hurst exponent.

The value of the Hurst index varies from 0 to 1. It is known that:

- A value of *H=0.5* indicates a truly random process and a completely uncorrelated series.
- A Hurst exponent value *H, 0.5 <H <1* indicates persistent behavior.
- A Hurst exponent value *0 <H <0.5* indicates anti-persistent behavior.
- An *H* closer to one indicates a high risk of large and abrupt changes.

It was calculated for all pixels of the whole study area using Detrended Fluctuation Analysis (DFA) in MATLAB® (Weron, 2011).

3.2.5. Sampling Method

To evaluate the performance of the presented key features, *EVI* samples from seven different land cover typologies (Fig. 1) were selected, and DWT analyses were applied for each of them.

EVI samples were selected randomly using NOAA's Biogeography Branch Sampling Design Tool (http://ccma.nos.noaa.gov/products/biogeography/sampling/) for each of the land cover vegetation classes. An irregular polygon was buffered around each sampling point, with a minimum number of 1500 pixels. The number of pixels for each polygon is defined using Efron's bootstrap method (Efron, 1979), with a confidence level of 95%. The average EVI of each sample of vegetation classes is used for DWT signal analysis. Furthermore, the selected key features have been applied to whole images by analysis of each pixel time-series signal to map and quantify the vegetation dynamics.

4. Results

4.1. Analysis of the Selected Vegetation Classes

The DWT decomposition components of EVI from 2003 to 2018 have been shown in Fig. 3. The stationary level of signals is given by the approximation series related to the low-frequency components (a_i), and noise or abnormal signals are given by the detailed series related to the high-frequency components (di).

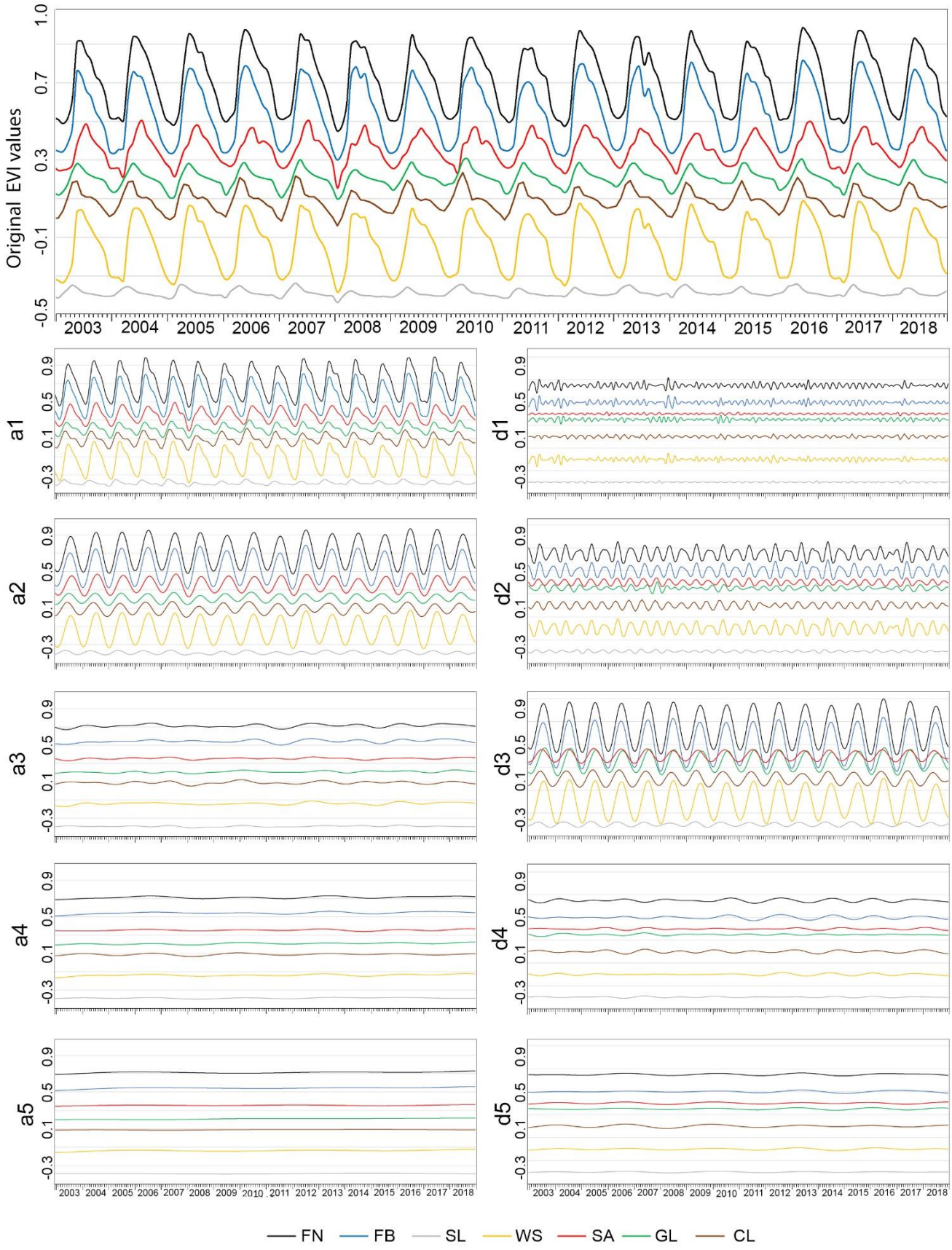

Figure 3. Original series (top) and discrete Wavelet Transform approximation (left) and details (right) components of MODIS *EVI* time series data using the 'dmey' wavelet function. The Y-axis values have shifted. FN: Needleleaf Forest, FB: Broadleaf Forest, SL: Closed Shrub, WS: Woody Savana, SA: Savanna, GL: Glass Land, CL: Crop Land.

The total intra-annual/seasonal variation *(Σv)* series and detail component level-3 have been shown in Fig 4. The d3 and *Σv* curves show similar trends and relatively equal amplitudes for all samples that describe the most volatility of total intra-annual variation. The maximum and minimum intra-annual variations for all vegetation were observed in mid-summer and early winter, respectively. The normalized wavelet variance was calculated to quantify the overall variability of *EVI* time-series data corresponding to DWT detail components (Fig. 4H). From 40% to 65% of the total variance of detail, components corresponds with detail component 3. The forests and woody savanna classes show the highest variability, and shrublands show the lowest in d3 components.

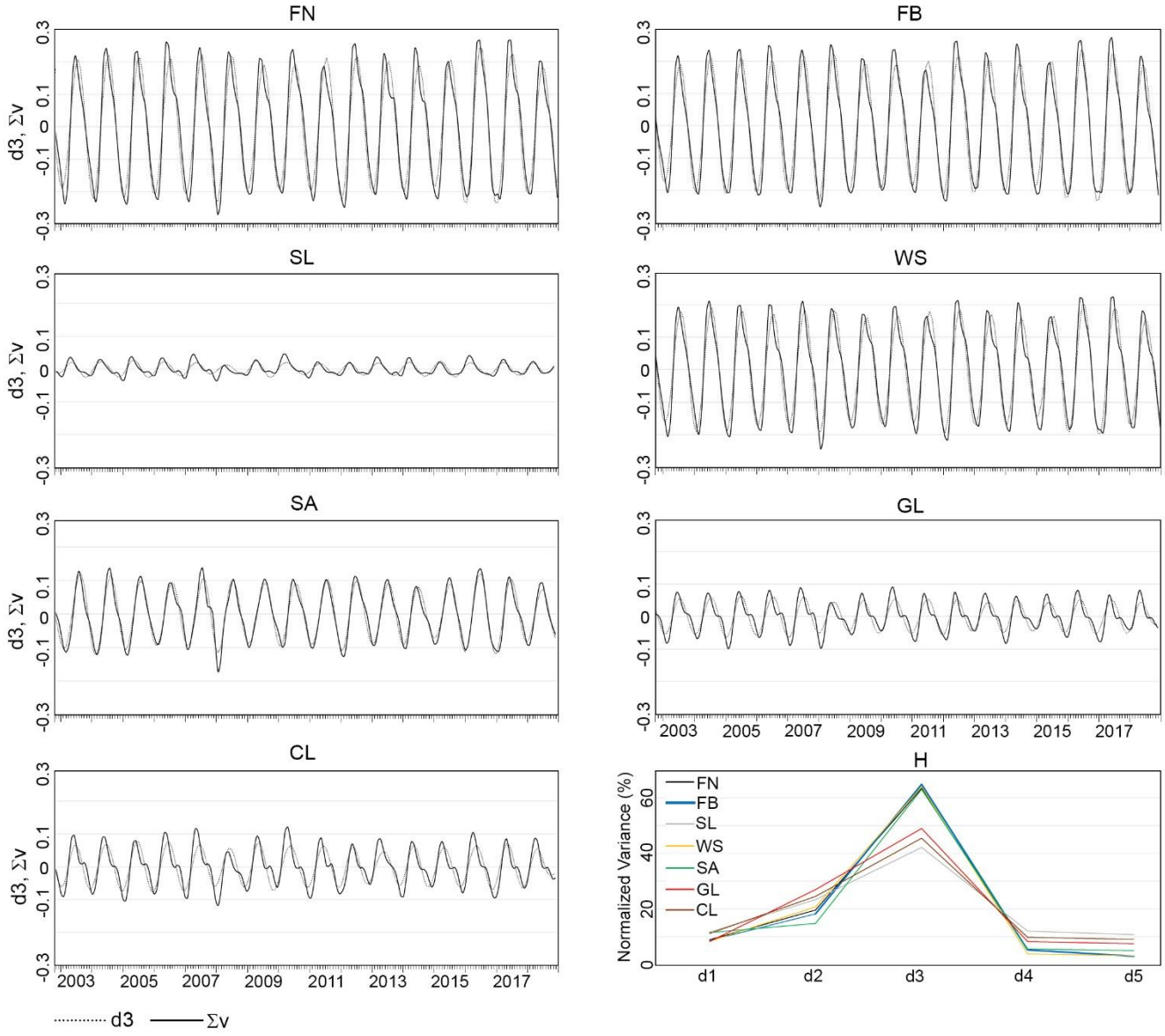

Figure 4. *EVI* time series of DWT detail component Level-3 (d3) (dashed line) and intra-annual total variation *(Σv)* (solid line) for FB: Broadleaf Forest, SL: Closed Shrub, WS: Woody Savana, SA: Savanna, GL: Glass Land, CL: Crop Land. H: Normalized variance versus DWT detail level *j* (j=1 to 5), for an average of vegetation samples.

The top 5 rows of Table 2 show the values of the key feature for the selected vegetation classes. High levels of vegetation cover are characterized by high values of EVImean and EVImin, and homogeneity is characterized by low ΔEVI. The maxima of the EVI series reach in July for savannas and late spring for the other vegetation classes.

Table 2. Statistical parameters were derived from the Mann-Kendall test, with a 5% confidence interval. (h=1: significant trend, h=0: non-significant trend. p-value<0.05 indicates a significant trend)

	Variable	FN	FB	SL	WS	SA	GL	CL
a5 (inter-annual) series	EVI_{mean}	0.3625	0.3428	0.1127	0.3622	0.3050	0.1083	0.1901
	EVI_{min}	0.1541	0.1391	0.0944	0.1832	0.2078	0.04571	0.1151
	ΔEVI	0.4199	0.4196	0.0458	0.3578	0.1953	0.1251	0.1535
	ΔEVI%	115.8	122.4	40.6	98.8	64.0	115.5	80.7
	t_{max}	June	June	May	June	July	June	May
	Tau-b	0.4045	0.5033	0.2072	0.4203	0.2429	0.7898	0.4915
	p-value	$< 10^{-5}$	$< 10^{-5}$	$< 10^{-5}$	$< 10^{-5}$	$< 10^{-5}$	$< 10^{-5}$	$< 10^{-5}$
	h	1	1	1	1	1	1	1
	Sen's slope ($*10^{-5}$)	9.2±1.1	9.4±1.7	2.1±0.8	8.7±1.7	3.1±1.1	8.8±0.5	3.3±0.4
	SU (%)	18.2	15.7	27.6	16.7	25.3	4.9	10.8
	CV	0.0222	0.0262	0.0265	0.0213	0.0134	0.0507	0.0137
	Hurst index	0.8440	0.9055	0.9950	0.8447	0.8715	1.0535	1.0042
Original EVI series	Mean	0.3625	0.3428	0.1126	0.3621	0.3050	0.1082	0.1899
	Tau-b	0.0185	0.0264	0.0538	0.0216	0.0123	0.0520	0.0031
	p-value	0.6994	0.5814	0.2609	0.6523	0.7985	0.2767	0.9487
	h	0	0	0	0	0	0	0
	Sen's slope ($*10^{-5}$)	4.7	7.0	2.0	6.5	2.3	5.7	0.3
	SU (%)	90.4	86.5	72.6	86.2	92.1	73.7	98.4
	CV	0.4385	0.4531	0.1607	0.3673	0.2447	0.4122	0.2925
	Hurst Index	0.3255	0.3420	0.5851	0.3120	0.3210	0.5002	0.4070

4.2. Trend Analysis

The approximation a5 component reveals the inter-annual changes, and therefore, its trend can display the long-term variation of the *EVI* series. Table 2 shows the statistical parameters of the Mann-Kendall test applied to the a5 component and original *EVI* series for the selected vegetation classes. The Kendal-Tau-b coefficient is a measure of rank correlation and shows the similarity of the orderings of data. The 100% negative and positive associations are expressed as +1 and -1, respectively (Agresti, 2010). This test was run by a confidence interval of 5%, by h coefficient, and, by two-sided p-values. The p-value is the probability that the data are randomly distributed rather than as a statistical trend. However, a p-value <0.05 indicates a significant trend (*h=1*). The Tau-b values for the original signals are around zero, which indicates a weak association to detect changes. Sen's slope has been used to quantify the magnitude of the trend. None of the original series display significant trends, and uncertainty in trend detection ranges from ~74% up to ~98%. In contrast, the slop uncertainties are considerably small for all 'a5' trends (~5.0% – ~25%), and all trends show significant association to detect changes.

4.3. Spatial Distribution of Vegetation Coverage

The top 5 rows of Table 2 presented key features that were calculated for all pixels to study vegetation dynamics and land cover changes during the period 2003-2018 in Iran. Fig. 5 shows EVI_{mean}, EVI_{min}, ΔEVI, and tmax images. The EVImean map (Fig. 5a) shows that the *EVI* amounts are high in the northern forest, and it is low in the center-north around the barren lands. The shrub and grasslands, which have occupied a vast area, have a low amount of *EVI*. The statistical classification of the EVImean values during the 2003-2018 period showed that the area with $EVI \leq 0.1$ accounted for 22.4%, the area with $0.1<EVI\leq0.2$ accounted for 30.1%, the area with $EVI > 0.2$ accounted for 4.6% of the total Iran area. The EVI_{min} (Fig. 5b) shows a similar pattern, and $EVI\leq0.1$ has the greatest area. The $\Delta EVI\%$ (Fig. 5c) shows that the north-west area and two patches in the north and west display high variations, and are not related to land cover types. Most of the whole pixels show a high *EVI* value in June-July (Fig. 5d). *EVI* peaks in winter, spring, summer, and, autumn are accounted for 7.5%, 30.2%, 20.6%, and 0.3% of the total area of Iran, respectively.

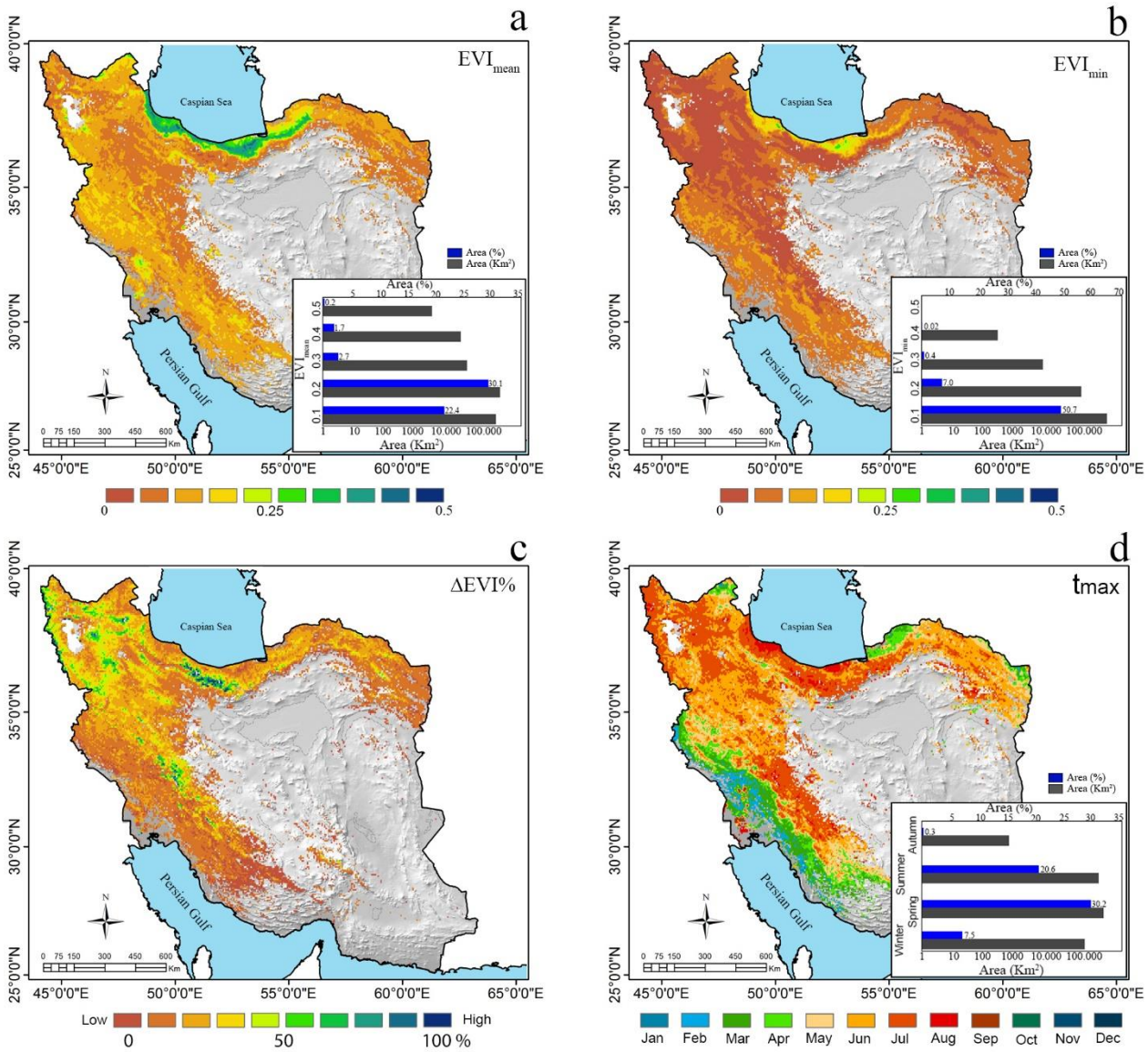

Figure 5. *EVI_{mean}(a), EVI_{min}(b), ΔEVI%(c)* and *EVI_{max} (d)* images derived from WT analysis

4.4. Variation of Vegetation Coverage

The coefficient of variation of *ΔEVI* (*CVEVI*) was calculated for all pixels as an index of the variability of the vegetation cover. The *CVEVI* ranges from zero up to 0.25 for the study area pixels.

In Fig.6 the image was classified into 5 categories: high variable *(0.25 ≤ CVEVI)*, relatively high variable *(0.15 ≤ CVEVI < 0.25)*, moderate variable *(0.10 ≤ CVEVI < 0.15)*, relatively low variable *(0.05 ≤ CVEVI < 0.10)*, and low variable *(CVEVI < 0.05)*. Areas with low and relatively low variability are dominant (~44%), and areas with relatively high and high volatility are distributed in small patches in the center and along the Persian Gulf coastlines.

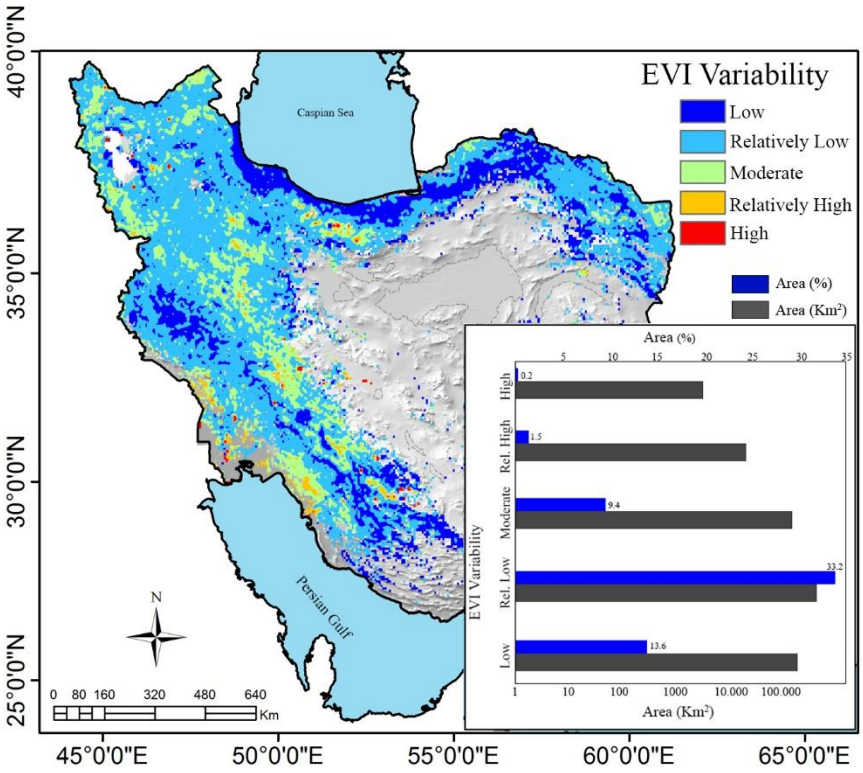

Figure 6. Coefficient of variation of the inter-annual *EVI* in Iran from 2003 to 2018.

The variation in trends of vegetation coverage is an important factor that displays the magnitude of land cover changes. Sen's slope is an effective index to characterize the magnitude of trends. The Sen's slope and Mann-Kendall test were applied to original signals and DWT approximation level-5 (a5) for all pixels to reveal the spatial distribution of variation in the trend of inter-annual *EVI* in the study area. The significance of trends for each of the pixels was checked. The value of *h=0* indicates that the slope is not significant, and the trend of variations is not valuable (Martínez & Gilabert, 2009). The Man-Kendall significance test (*h*) reveals whether the observed slope is significant or not, and a value of *h=0* shows that there is no trend. As shown in Fig. 7a, more than 33% of the original series has *h=0*, while the a5 series have only 7.8% of non-significant pixels. Therefore, the a5 series per pixel were used to analyze data series trends and, pixels with *h=0* were masked (Fig. 7c). The center and northwest areas show positive trends, and the southwest and northeast display negative trends. Jiang et al. (2015) have used Sens's slope and Mann-Kendall test Z score to classify the trends variation of vegetation in the Yellow River Basin. Here, the same methodology was used to classify variation of land cover vegetation of the study area as degradation, stability, and improvement. The Hurst exponent results for DWT 'a5' component were considered to describe the sustainability of inter-annual variations. The Hurst exponent of all pixels is 0.5 on average. The pixels with Hurst exponent <0.5 are sustainable, and those higher than 0.5 are unsustainable (Fig. 7b). The sustainable and unsustainable regions account for 89.0% and 11.0% of the total vegetated area, respectively. However, regions with sustainable trend variation were considered for trend analysis and the remainings were masked. The Mann-Kendal test was run at a confidence level of 0.05, and classes were defined as significant variations *($Z > 1.9$ or $Z < -1.9$)* or insignificant variations *($-1.9 \leq Z \leq 1.9$)* (Fig. 7d). The improved vegetation covers are distributed in the north, north-west, north-east, east, and center of Iran, whereas, the slight and, severely degraded vegetation areas are located in the north-east and south-west. More than 14% of land cover are subject to stable vegetation trend, ~5.5% is under degradation, and ~37.7% show improved trends.

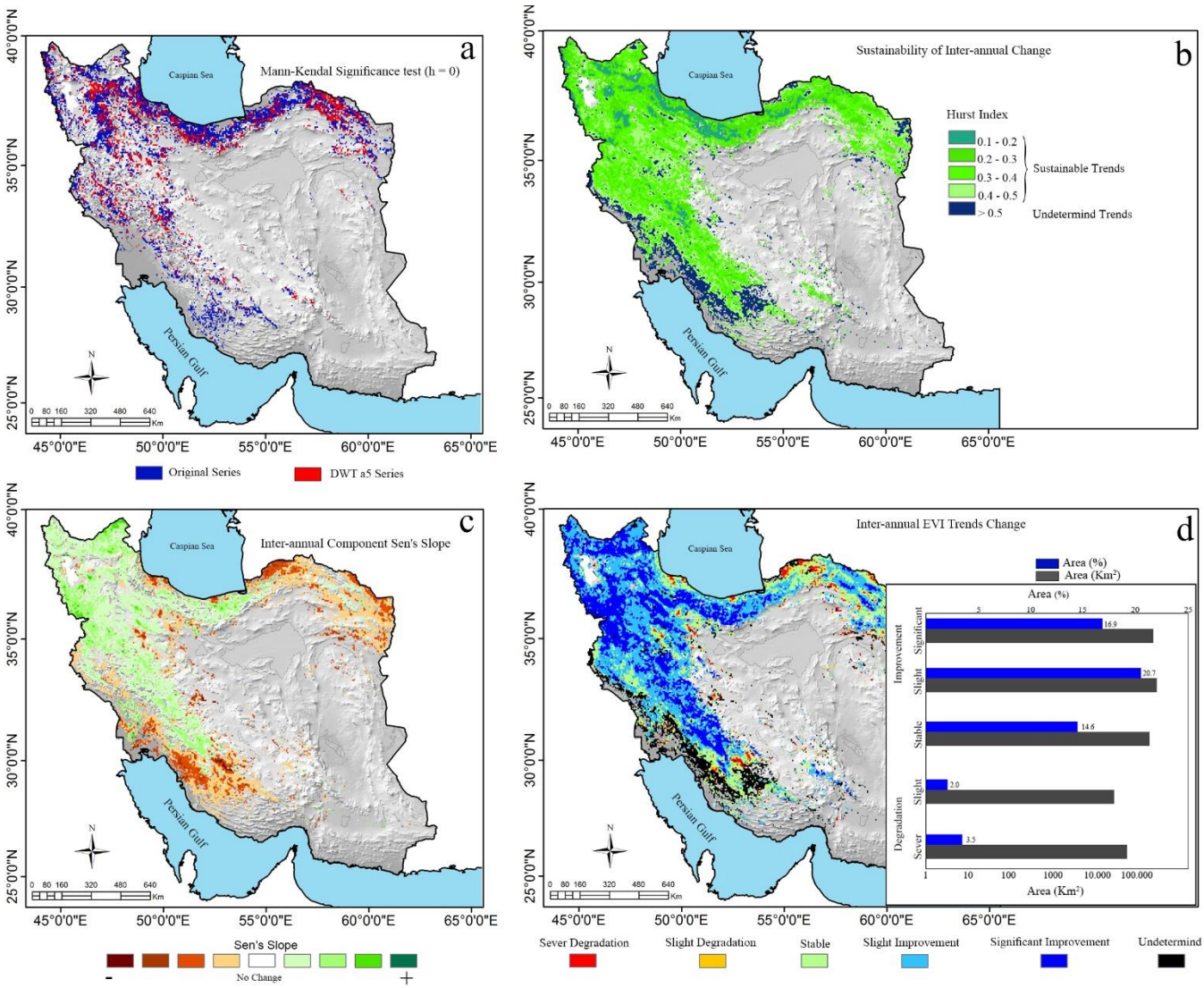

Figure 7. a) image of non-significant pixels (*h=0*) from Mann-Kendall test for inter-annual components (DWT a5), and original *EVI* signals. b) sustainability of inter-annual trends from Hurst exponent. Pixels with values larger than 0.5 show unsustainable trends. c) Sen's Slope (Magnitude of vegetation change) image over Iran. d) Spatial distribution of the inter-annual EVI trends

5. Discussion

5.1. Variations in Vegetation Index Over Time

Seasonal and inter-annual variations of vegetation indices characterize the phenological dynamics and in long-term series lead to understanding the land cover change (Cai & Yu, 2009; Fan et al., 2012; Lambin et al., 2003). WT is a powerful method for time-series data analysis that decomposes an original signal into stationary and non-stationary components. It has been used widely to understand the inter-annual and phenological cycles, change detection, and correlation between phenology and meteorological factors from vegetation index time series data (Bruce et al., 2006; Carl et al., 2013; Moreira et al., 2019; Percival et al., 2004; Piao et al., 2012). The stability and abnormality of the *EVI* series refer to vegetation dynamics at different time scales. However, the scale and frequency of WT signals are the most important factors to exactly reveal the Spatiotemporal variations. The stationary level of the original signal is given by the low-frequency components, and non-stationary or abnormal elements are related to the high-frequency components. The first level of DWT components of MODIS 16-day composite L3 products was identified as sub-monthly noise, and it was ignored. The detail level-3 (d3) refers to seasonal changes and is related to vegetation phenology. It was shown that the sum of detail components level-2 up to level-5 represents the total intra-annual variability. The 5th approximation component (a_5) is linked to the inter-annual variations and shows relatively flat curves for all vegetation classes.

5.2. Temporal Trends in Vegetation between 2003 and 2018

The trend of vegetation variations is an important factor for understanding the land cover changes. The non-

parametric Sen's Slope analysis, together with the Man-Kendall test was applied to analyze the trend of inter-annual and intra-annual series. The combination of these two methods for trend analysis of vegetation indexes (EVI and NDVI) is more advantageous than the other statistical methods such as linear regression, and have been tested in some different regions (Cai & Yu, 2009; Jiang et al., 2015; Martínez & Gilabert, 2009). Therefore, areas that show a significant trend of vegetation variations are considered for land cover change detection. Furthermore, the Hurst exponent was used to characterize the sustainability of the trend of vegetation time-series signals. The sustainability of trends improves the results of land cover changes, and it could be an index for future land cover change prediction.

5.3. Spatio-Temporal Patterns

The result of the d_3 component (semi-period ~90 days) profile shows the highest and lowest peaks in summer (late July-August) and winter (late December-January) respectively, which corresponds to the photosynthetic activity of vegetation classes (Nasiri et al., 2004; Reykande et al., 2013). The d_3 components show absolute EVI maximum value in late spring and early summer for all of the selected vegetation classes, which corresponds to the photosynthetic activity of all of the selected vegetation classes, and the corresponding dates could be considered as the date of maximum EVI (t_{max}).

The average vegetation amount during the reported period is characterized by inter-annual curves (a5). The forests show the highest, and closed shrublands show the lowest average of EVI. All of the inter-annual curves are relatively flat, and small peaks were observed in 2004- 2005. Also, small troughs were present in 2009-2010 for all vegetation classes profile, except croplands and grasslands. These results are consistent with the Eskandari et al. (2021) research, which states that at a nationwide, annual scale, trends in vegetation indices have not changed significantly over the 15-year study period. However, no critical variations were observed in the EVI inter-annual profiles for the selected classes, and relatively flat trends were estimated. The closed shrub and savanna land covers show more homogenous vegetation, and forests and woody savanna show the highest level of vegetation.

The seasonal changes appear in d_3 components which have values greater than eighty percent (*ΔEVI% >80%)*. The closed shrub covers are characterized by low EVI_{mean}, EVI_{min}, and *ΔEVI%* values, which indicate its phenological cycles are not related to seasonal cycles and depend on other parameters like precipitation amounts. Whereas, the crop and grasslands display low vegetation levels and high value of variations.

All selected vegetation classes show positive trends which are not significant in original signals. The southwest part has an arid climate and also shows a low value of *EVI*. The small patches of vegetation with high *EVI* values were observed in croplands (e.g. northwest). The *ΔEVI%* shows that the northwest area and two patches in the north and west display high variations, and are not related to land cover types. Most of the whole pixels show a high *EVI* value in June-July. The central areas show *EVI* peaks in late-spring early-summer, which corresponds to the photosynthetic activity, and spring peaks and winter peaks are present in the north and south-west areas, respectively, which corresponds to the climatic conditions of the region.

The mid-late winter peaks are located on the north and along the Persian Gulf coasts, which correspond to shrublands and crop areas. Vegetation changes along the Persian Gulf coastline undergo usually start sooner during the year, and this area is covered by herbs in early winter and is cultivated in late winter. Forests reach EVI_{max} during June and July. Most of the irrigated areas show maximum *EVI* in August. All forests show low variability of vegetation index. It can be concluded that the vegetation coverage is stable in the whole study area. Forests mainly show positive trends, and small patches of cultivated areas in the southern Caspian Sea show negative trends. The areas with negative values are subject to losses of vegetation due to land cover changes.

6. Summary and Conclusion

In this research, the remote sensing data was applied to assess the Spatio-temporal variability of vegetation across Iran for the period 2003–2018. The *EVI* time series data from MODIS Terra Level-3 products at a resolution of 1km were downloaded. The *EVI* data sets were sampled from 7 vegetation typologies based on MODIS land cover yearly data. The *EVI* temporal signals were smoothed, gaps filled, and monthly maximum value composites were created. The average *EVI* of each vegetation class sample was used for data analysis. DWT, Variation Coefficient, Sens's Slope trend analysis, and Hurst exponent were applied to *EVI* samples to investigate the temporal variations, suitable key features, and, quantitative indexes for whole image Spatio-temporal analysis. It was concluded that the DWT reduces the dispersion of *EVI* time-series signals, and therefore the temporal analysis of the WT components series could be more effective than of the original series. The EVI_{mean}, EVI_{min}, *ΔEVI*, EVI_{max}, and trends of variations were calculated for whole images based on per pixel. The following results were obtained in the study area:

- Bare lands cover more than 58% of the total area of Iran. Vegetation coverage of Iran is distributed in the north, north-west, west, south-west, and, north-east, and no effective trends is observed in *EVI* values. The forests (in the north) show the highest, and closed shrublands show the lowest average of *EVI* values.

- The inter-annual average of *EVI* of vegetation classes varies from 0.1 to 0.36 during 2003-2018. The variations of the inter-annual series did not present a significant trend, and a relatively flat curve was observed for all vegetation classes. However, small troughs and peaks (±0.1 of *EVI* value) appear in 2009-2010 and 2004-2005, respectively. The highest degree of intra-annual variations is due to seasonal phenological cycles, and it is the major source of variations. The maximum and minimum values of intra-annual variations were observed in mid-summer and early winter, respectively. Spatially, the highest degree of variations is located in the north and northwest as small patches, which are not related to land cover types. The area of vegetation coverage of *EVI* maximum is 7.5% in winter, 30.2% in spring, 20.6% in summer, and 0.3% in autumn.
- The vegetation coverage was stable at 44% and varied with a large amplitude in 1.7% of the total area of Iran. About 89% of vegetation coverage is under sustainable variations. Although most of the regions show positive changes, some areas are under negative changes (degradation), i.e. loss of vegetation coverage. The regions with improved vegetation coverage are located in the north, west, and, south-west and account for 37.7% of the total area. Vegetation coverages that are under degradation are distributed in the north-east and south-west, and their area is 5.5% of the total area.

In summary, WT and statistical methods were used to identify the Spatio-temporal variations and trends of the vegetation index of Iran. These methodologies enable us to define land cover changes. However, the performance of WT and Mann-Kendall tests depends on datasets. Here, more than 15 years of data series of *EVI* were used for vegetation variations assessment in Iran. This time range may limit the accuracy of results about land cover changes and the trend of variations. It is suggested to use longer time-series datasets (e.g. 30-years) such as AVHRR EVI/NDVI from Global Inventory Modelling and Mapping Studies (GIMMS) in combination with MODIS vegetation index.

References

Abdi, O., Shirvani, Z., & Buchroithner, M. F. (2018). Spatiotemporal drought evaluation of Hyrcanian deciduous forests and semi-steppe rangelands using moderate resolution imaging spectroradiometer time series in Northeast Iran. Land Degradation & Development, 29(8), 2525–2541.

Agresti, A. (2010). Analysis of Ordinal Categorical Data. John Wiley & Sons.

Ahmadi, H., & Nusrath, A. (2010). Vegetation change detection of Neka River in Iran by using remote-sensing and GIS. Journal of Geography and Geology, 2(1), 58.

Amiri, R., Weng, Q., Alimohammadi, A., & Alavipanah, S. K. (2009). Spatial–temporal dynamics of land surface temperature in relation to fractional vegetation cover and land use/cover in the Tabriz urban area, Iran. Remote Sensing of Environment, 113(12), 2606–2617.

Bashmachnikov, I., Belonenko, T. V., & Koldunov, A. V. (2013). Intra-annual and interannual non-stationary cycles of chlorophyll concentration in the Northeast Atlantic. Remote Sensing of Environment, 137. https://doi.org/10.1016/j.rse.2013.05.025

Beck, P. S. A., Atzberger, C., Høgda, K. A., Johansen, B., & Skidmore, A. K. (2006). Improved monitoring of vegetation dynamics at very high latitudes: A new method using MODIS NDVI. Remote Sensing of Environment, 100(3), 321–334. https://doi.org/10.1016/j.rse.2005.10.021

Bradley, B. A., Jacob, R. W., Hermance, J. F., & Mustard, J. F. (2007). A curve fitting procedure to derive inter-annual phenologies from time series of noisy satellite NDVI data. Remote Sensing of Environment, 106(2), 137–145.

Bruce, L. M., Mathur, A., & Byrd, J. (2006). Denoising and wavelet-based feature extraction of MODIS multi-temporal vegetation signatures. GIScience & Remote Sensing, 43(1), 67–77.

Cai, B. F., & Yu, R. (2009). Advance and evaluation in the long time series vegetation trends research based on remote sensing. J. Remote Sens, 13(6), 1170–1186.

Cao, R., Chen, J., Shen, M., & Tang, Y. (2015). An improved logistic method for detecting spring vegetation phenology in grasslands from MODIS EVI time-series data. Agricultural and Forest Meteorology, 200, 9–20.

Carl, G., Doktor, D., Koslowsky, D., & Kühn, I. (2013). Phase difference analysis of temperature and vegetation phenology for beech forest: A wavelet approach. Stochastic Environmental Research and Risk Assessment, 27(5), 1221–1230.

Cihlar, J., St.-Laurent, L., & Dyer, J. A. (1991). Relation between the normalized difference vegetation index and ecological variables. Remote Sensing of Environment, 35(2), 279–298. https://doi.org/10.1016/0034-4257(91)90018-2

De Beurs, K. M., & Henebry, G. M. (2005). A statistical framework for the analysis of long image time series. International Journal of Remote Sensing, 26(8), 1551–1573.

Detsch, F., Otte, I., Appelhans, T., Hemp, A., & Nauss, T. (2016). Seasonal and long-term vegetation dynamics from 1-km GIMMS-based NDVI time series at Mt. Kilimanjaro, Tanzania. Remote Sensing of Environment, 178, 70–83. https://doi.org/10.1016/j.rse.2016.03.007

Detsch, F., Otte, I., Appelhans, T., & Nauss, T. (2016). A comparative study of cross-product NDVI dynamics in the

Kilimanjaro region—A matter of sensor, degradation calibration, and significance. Remote Sensing, 8(2), 159.

Didan, K. (2015). MYD13A1 MODIS/Aqua Vegetation Indices 16-day L3 Global 500m SIN Grid V006 [Data set]. NASA EOSDIS LP DAAC. 10.5067/MODIS/MYD13A1.006

Echer, E. (2004). Multi-resolution analysis of global total ozone column during 1979?1992 Nimbus-7 TOMS period. Annales Geophysicae, 22(5), 1487–1493.

Eerens, H., Haesen, D., Rembold, F., Urbano, F., Tote, C., & Bydekerke, L. (2014). Image time series processing for agriculture monitoring. Environmental Modelling & Software, 53, 154–162. https://doi.org/10.1016/j.envsoft.2013.10.021

Efron, B. (1979). Bootstrap methods: Another look at the jackknife. In Breakthroughs in statistics (pp. 569–593). Springer.

Emadodin, I., Narita, D., & Bork, H. R. (2012). Soil degradation and agricultural sustainability: An overview from Iran. Environment, Development and Sustainability, 14(5), 611–625.

Eftekhari, T., Ramezani, M., 2004. Introduction to Plant Biodiversity in Iran. In: Biodiversity and Medicinal Plant Wealth of South Asian Countries. (eds). P. Pushpangadan, K.N. Nair and M.R. Ahmad P.39-40. National Botanical Research Institute, Lucknow-226001,India.

Eskandari Dameneh, H., Gholami, H., Telfer, M.W. et al. Desertification of Iran in the early twenty-first century: assessment using climate and vegetation indices. Sci Rep 11, 20548 (2021). https://doi.org/10.1038/s41598-021-99636-8.

Fan, N., Xie, G. D., Zhang, C. S., Chen, L., Li, W. H., & Cheng, S. K. (2012). Spatial-temporal dynamic changes of vegetation cover in Lancang River Basin during 2001–2010. Resources Science, 34(7), 1222–1231.

Fensholt, R., & Proud, S. R. (2012). Evaluation of Earth Observation based global long term vegetation trends—Comparing GIMMS and MODIS global NDVI time series. Remote Sensing of Environment, 119, 131–147. https://doi.org/10.1016/j.rse.2011.12.015

Fensholt, R., Rasmussen, K., Nielsen, T. T., & Mbow, C. (2009). Evaluation of earth observation based long term vegetation trends—Intercomparing NDVI time series trend analysis consistency of Sahel from AVHRR GIMMS, Terra MODIS and SPOT VGT data. Remote Sensing of Environment, 113(9), 1886–1898.

Freitas, R. M., & Shimabukuro, Y. (2008). Combining wavelets and linear spectral mixture model for MODIS satellite sensor time-series analysis. Journal of Computational Interdisciplinary Sciences, 1, 33–38.

Friedl, M. A., Sulla-Menashe, D., Tan, B., Schneider, A., Ramankutty, N., Sibley, A., & Huang, X. (2010). MODIS Collection 5 global land cover: Algorithm refinements and characterization of new datasets. Remote Sensing of Environment, 114(1), 168–182.

Fu, X., Tang, C., Zhang, X., Fu, J., & Jiang, D. (2014). An improved indicator of simulated grassland production based on MODIS NDVI and GPP data: A case study in the Sichuan province, China. Ecological Indicators, 40, 102–108. https://doi.org/10.1016/j.ecolind.2014.01.015

Garcia, D. (2010). Robust smoothing of gridded data in one and higher dimensions with missing values. Computational Statistics and Data Analysis, 54(4). https://doi.org/10.1016/j.csda.2009.09.020

Golian, S., Mazdiyasni, O., & AghaKouchak, A. (2015). Trends in meteorological and agricultural droughts in Iran. Theoretical and Applied Climatology, 119(3–4), 679–688.

Hawinkel, P., Swinnen, E., Lhermitte, S., Verbist, B., Van Orshoven, J., & Muys, B. (2015). A time series processing tool to extract climate-driven interannual vegetation dynamics using Ensemble Empirical Mode Decomposition (EEMD). Remote Sensing of Environment, 169, 375–389. https://doi.org/10.1016/j.rse.2015.08.024

Heshmati, G.A., 2012. Vegetation characteristics of four ecological zones of Iran. Int. J. Plant Prod. 1, 215–224.

Higginbottom, T., Symeonakis, E., 2014. Assessing land degradation and desertification using vegetation index data: Current frameworks and future directions. Remote Sens. 6, 9552–9575.

Hou, X., Wu, T., Yu, L., & Qian, S. (2012). Characteristics of multi-temporal scale variation of vegetation coverage in the Circum Bohai Bay Region, 1999–2009. Acta Ecologica Sinica, 32(6), 297–304.

Huete, A., Didan, K., Miura, T., Rodriguez, E. P., Gao, X., & Ferreira, L. G. (2002). Overview of the radiometric and biophysical performance of the MODIS vegetation indices. Remote Sensing of Environment, 83(1–2), 195–213.

Hurst, H. E. (1951). Long-term storage capacity of reservoirs. Trans. Amer. Soc. Civil Eng., 116, 770–799.

Hyndman, R. J., Athanasopoulos, G., Bergmeir, C., Caceres, G., Chhay, L., O'Hara-Wild, M., Petropoulos, F., Razbash, S., Wang, E., & Yasmeen, F. (2018). forecast: Forecasting functions for time series and linear models. https://researchportal.bath.ac.uk/en/publications/forecast-forecasting-functions-for-time-series-and-linear-models

Jiang, W., Yuan, L., Wang, W., Cao, R., Zhang, Y., & Shen, W. (2015). Spatio-temporal analysis of vegetation variation in the Yellow River Basin. Ecological Indicators, 51, 117–126. https://doi.org/10.1016/j.ecolind.2014.07.031

Kazemzadeh, M., & Malekian, A. (2016). Spatial characteristics and temporal trends of meteorological and hydrological droughts in northwestern Iran. Natural Hazards, 80(1), 191–210.

Lambin, E. F., Geist, H. J., & Lepers, E. (2003). Dynamics of land-use and land-cover change in tropical regions.

Annual Review of Environment and Resources, 28(1), 205–241.

Lunetta, R. S., Knight, J. F., Ediriwickrema, J., Lyon, J. G., & Worthy, L. D. (2006). Land-cover change detection using multi-temporal MODIS NDVI data. Remote Sensing of Environment, 105(2), 142–154.

Madani, K., AghaKouchak, A., & Mirchi, A. (2016). Iran's socio-economic drought: Challenges of a water-bankrupt nation. Iranian Studies, 49(6), 997–1016.

Martínez, B., & Gilabert, M. A. (2009). Vegetation dynamics from NDVI time series analysis using the wavelet transform. Remote Sensing of Environment, 113(9), 1823–1842. https://doi.org/10.1016/j.rse.2009.04.016

Meyer, Y. (1993). Wavelets—Algorithms and applications. http://adsabs.harvard.edu/abs/1993waa..book.....M

Modarres, R., da Silva, V. de P.R., 2007. Rainfall trends in arid and semi-arid regions of Iran. J. Arid Environ. 70, 344–355.

Moreira, A., Fontana, D. C., & Kuplich, T. M. (2019). Wavelet approach applied to EVI/MODIS time series and meteorological data. ISPRS Journal of Photogrammetry and Remote Sensing, 147, 335–344.

Nasiri, M., Mohaddesi, A., & Amani, R. (2004). Study of growth pattern and determination of growth stages in rice varieties. http://agris.fao.org/agris-search/search.do?recordID=IR2006000360

Pan, Y., Li, L., Zhang, J., Liang, S., Zhu, X., & Sulla-Menashe, D. (2012). Winter wheat area estimation from MODIS-EVI time series data using the Crop Proportion Phenology Index. Remote Sensing of Environment, 119, 232–242.

Peng, J., Liu, Z., Liu, Y., Wu, J., & Han, Y. (2012). Trend analysis of vegetation dynamics in Qinghai–Tibet Plateau using Hurst Exponent. Ecological Indicators, 14(1), 28–39.

Percival, D. B., & Walden, A. T. (2006). Wavelet Methods for Time Series Analysis. Cambridge University Press.

Percival, D. B., Wang, M., & Overland, J. E. (2004). An introduction to wavelet analysis with applications to vegetation time series. Community Ecology, 5(1), 19–30.

Piao, Y., Yan, B., Guo, S., Guan, Y., Li, J., & Cai, D. (2012). Change detection of MODIS time series using a wavelet transform. 2012 International Conference on Systems and Informatics (ICSAI2012), 2093–2097.

Rahimi, J., Ebrahimpour, M., & Khalili, A. (2013). Spatial changes of extended De Martonne climatic zones affected by climate change in Iran. Theoretical and Applied Climatology, 112(3–4), 409–418.

Reykande, J. K., Amiri, N. A., & Shahabian, M. (2013). Analyzing phenological stages of three citrus varieties at foothills, plain and shoreline areas of Sari in North of Iran. International Journal of Agriculture and Crop Sciences, 6(8), 452.

Rocha, A. V., & Shaver, G. R. (2009). Advantages of a two band EVI calculated from solar and photosynthetically active radiation fluxes. Agricultural and Forest Meteorology, 149(9), 1560–1563.

Roerink, G. J., Menenti, M., Soepboer, W., & Su, Z. (2003). Assessment of climate impact on vegetation dynamics by using remote sensing. Physics and Chemistry of the Earth, Parts A/B/C, 28(1), 103–109. https://doi.org/10.1016/S1474-7065(03)00011-1

Sagheb-Talebi, K., Sajedi, T., & Pourhashemi, M. (2014). Forests of Iran: A Treasure from the Past, a Hope for the Future. Springer Science & Business Media.

Shuang-cheng, L. I., Zhi-qiang, Z., Yang, G., & Yang-lin, W. (2008). Determining the predictability and the spatial pattern of urban vegetation using recurrence quantification analysis: A case study of Shenzhen City. 地理研究, 27(6), 1243–1252.

Sims, D. A., Rahman, A. F., Cordova, V. D., El-Masri, B. Z., Baldocchi, D. D., Flanagan, L. B., Goldstein, A. H., Hollinger, D. Y., Misson, L., & Monson, R. K. (2006). On the use of MODIS EVI to assess gross primary productivity of North American ecosystems. Journal of Geophysical Research: Biogeosciences, 111(G4).

Song, F.Q., Xing, K.X., Liu, Y., Liu, Z.C., & Kang, M.Y. (2011). Monitoring and assessment of vegetation variation in Northern Shaanxi based on MODIS/NDVI. Acta Ecologica Sinica, 3(2), 354–363.

Swets, D., Reed, B. C., Rowland, J., & Marko, S. E. (1999). A weighted least-squares approach to temporal NDVI smoothing. From image to information: 1999 ASPRS Annual Conference. https://pubs.er.usgs.gov/publication/70201050

Tan, B., Morisette, J. T., Wolfe, R. E., Gao, F., Ederer, G. A., Nightingale, J., & Pedelty, J. A. (2011). An enhanced TIMESAT algorithm for estimating vegetation phenology metrics from MODIS data. IEEE Journal of Selected Topics in Applied Earth Observations and Remote Sensing, 4(2), 361–371.

Tucker, C. J., Newcomb, W. W., Los, S. O., & Prince, S. D. (1991). Mean and inter-year variation of growing-season normalized difference vegetation index for the Sahel 1981-1989. International Journal of Remote Sensing, 12(6), 1133–1135.

Van Leeuwen, M., Coops, N. C., Hilker, T., Wulder, M. A., Newnham, G. J., & Culvenor, D. S. (2013). Automated reconstruction of tree and canopy structure for modeling the internal canopy radiation regime. Remote Sensing of Environment, 136, 286–300.

Wang, G., Garcia, D., Liu, Y., de Jeu, R., & Johannes Dolman, A. (2012). A three-dimensional gap filling method for large geophysical datasets: Application to global satellite soil moisture observations. Environmental Modelling and Software, 30. https://doi.org/10.1016/j.envsoft.2011.10.015

Weron, R. (2011). DFA: MATLAB function to compute the Hurst exponent using Detrended Fluctuation Analysis (DFA). HSC Software.

Wessels, K.J., Prince, S.D., Reshef, I., 2008. Mapping land degradation by comparison of vegetation production to spatially derived estimates of potential production. J. Arid Environ. 72, 1940–1949.

Wessels, K.J., Van Den Bergh, F., Scholes, R.J., 2012. Limits to detectability of land degradation by trend analysis of vegetation index data. Remote Sens. Environ. 125, 10–22.

Zhang, X., Friedl, M. A., Schaaf, C. B., Strahler, A. H., Hodges, J. C., Gao, F., Reed, B. C., & Huete, A. (2003). Monitoring vegetation phenology using MODIS. Remote Sensing of Environment, 84(3), 471–475.

Zhang, Y., Song, C., Band, L. E., Sun, G., & Li, J. (2017). Reanalysis of global terrestrial vegetation trends from MODIS products: Browning or greening? Remote Sensing of Environment, 191, 145–155.

Zhang, Y., Xu, M., Chen, H., & Adams, J. (2009). Global pattern of NPP to GPP ratio derived from MODIS data: Effects of ecosystem type, geographical location and climate. Global Ecology and Biogeography, 18(3), 280–290.

Zhao, M., Heinsch, F. A., Nemani, R. R., & Running, S. W. (2005). Improvements of the MODIS terrestrial gross and net primary production global data set. Remote Sensing of Environment, 95(2), 164–176.

Ziegel, E., Press, W., Flannery, B., Teukolsky, S., & Vetterling, W. (1987). Numerical Recipes: The Art of Scientific Computing. Technometrics, 29(4). https://doi.org/10.2307/1269484

Zoljoodi, M., & Didevarasl, A. (2013). Evaluation of spatial–temporal variability of drought events in Iran using palmer drought severity index and its principal factors (through 1951–2005). Atmos Clim Sci, 3, 193–207.